in vivo *27*: 339-350 (2013)

Simultaneous Imaging of Temporal Changes of NF-κB Activity and Viable Tumor Cells in Huh7/NF-κB-*tk-luc2*/*rfp* Tumor-bearing Mice

WEI-HSUN WANG[1,2*], I-TSANG CHIANG[1*], YU-CHANG LIU[1,3], FEI-TING HSU[1], HONG-WEN CHEN[4], CHUAN-LIN CHEN[1], YI-JANG LEE[1], WUU-JYH LIN[5] and JENG-JONG HWANG[1]

[1]*Departments of Biomedical Imaging and Radiological Sciences, National Yang-Ming University, Taipei, Taiwan, R.O.C.;*
[2]*Orthopedic Surgery, Changhua Christian Hospital, Changhua, Taiwan, R.O.C.;*
[3]*Department of Radiation Oncology, National Yang-Ming University Hospital, Yilan, Taiwan, R.O.C.;*
[4]*Department of Radiation Oncology and Hospice Care Center, Mackay Memorial Hospital, Taipei, Taiwan, R.O.C.;*
[5]*Division of Radioisotope, Institute of Nuclear Energy Research, Taoyuan, Taiwan, R.O.C.*

Abstract. *Few studies have reported that the effect of sorafenib on advanced human hepatocellular carcinoma (HCC) is taking place via the inhibition of NF-κB signal transduction. Here we constructed a human HCC Huh7 stable clone with NF-κB-responsive element to drive dual reporter genes, herpes simplex virus thymidine kinase (tk) and firefly luciferase (luc2), and co-transfected with a third red fluorescent protein (rfp) gene, renamed as Huh7/NF-κB-tk-luc2/rfp cells, and combined with bioluminescent imaging (BLI) and red fluorescent protein imaging (RFPI) to monitor the effect of sorafenib on NF-κB activation and tumor inhibition. The results show that sorafenib could suppress the NF–κB-DNA binding activity, and the expression of downstream effector proteins. Notably, the relative photon fluxes obtained from RFPI and BLI, which represent the viable tumor cells and cells with NF-κB activation, decreased after sorafenib treatment by 50 to 65%, and 87.5 to >90%, respectively, suggesting that NF-κB activation is suppressed in viable HCC cells by sorafenib. Simultaneous molecular imaging of the temporal change of NF-κB activity and of viable cells in the same Huh7/NF-κB-tk-luc2/rfp tumors of the animal may reflect the real status of NF-κB activity and the viable tumor cells at the time of imaging.*

Liver cancer, comprised mainly of hepatocellular carcinoma (HCC), is ranked fourth in cancer mortality worldwide (1). Disease recurrence after curative treatment and progression after non-curative intervention are common, with a poor prognosis (2, 3). Hepatocarcinogenesis is related to dysregulated apoptosis, which may also be the main reason for treatment failure in patients with HCC (4). Nuclear factor-kappaB (NF-κB) is a transcription factor governing the expression of more than 400 genes. Among these, genes related to inflammatory processes, cell cycle, apoptosis and cancer cell invasion/metastasis are of particular investigational interest, aimed at solving anticancer treatment resistance (5).

The classical NF-κB pathway is frequently activated in human HCC and non-tumorous adjacent tissues and HCC cell lines (6). Oncogenesis of chronic hepatitis, in which constitutional activation of NF-κB in hepatocytes is triggered by tumor necrosis factor-α from surrounding endothelial and inflammatory cells, has been reported (7). Aberrant expression of cyclin-D1, which controls cell-cycle progression and leads to the increased proliferation of HCC cells, can be inhibited by blocking of the NF-κB signaling pathway (8). Other NF-κB-regulated downstream cytokines/proteins have also been reported. Overexpression of B-cell lymphoma-2 (BCL-2) and X-linked inhibitor of apoptosis protein (XIAP), both anti-apoptotic proteins, can be inhibited in HCC cells through the suppression of cytokine-associated NF-κB activation (9, 10). Vascular endothelial growth factor (VEGF), a prognostic factor for poor survival in patients with HCC (11, 12), can induce angiogenesis in mouse hepatoma-derived endothelial

*These Authors contributed equally to this study.

Correspondence to: Jeng-Jong Hwang, Department of Biomedical Imaging and Radiological Sciences, National Yang-Ming University, Taipei, Taiwan, No. 155, Sec. 2, Li-Nong St., Bei-tou, Taipei 112, Taiwan, R.O.C. Tel: +886 228267064, Fax: +886 228201095, email: jjhwang@ym.edu.tw

Key Words: Human hepatocellular carcinoma, sorafenib, temporal NF-κB monitoring, RFP, imaging.

cells *via* NF-κB/the serine-threonine kinase Akt (also known as protein kinase B, PKB) pathway (13). Matrix metalloproteinase-9 (MMP-9) degrades extracellular matrix proteins, and is associated with the invasive capability of HCC (14, 15). Both VEGF and MMP-9 can be down-regulated *via* the suppression of NF-κB, and result in reduced angiogenesis and invasion of HCC cells (6, 13, 15, 16). As a consequence, the molecular processes in HCC development and the response to specific anti-HCC therapy might be evaluated based on the expressions of NF-κB-regulated genes (17, 18).

The NF-κB activity can be assessed by immunohistochemical (IHC) staining, electrophoretic mobility shift assay (EMSA) for nuclear translocalization, or protein–DNA binding. However, neither EMSA nor IHC staining is adequate to represent the NF-κB activity at the transcriptional level. In addition, animals need to be sacrificed in order to obtain tissue samples for analysis, and the methods involved are not only time consuming and laborious (19), but also only represent the NF-κB status of the region not of the whole tumor.

Hypermethylation and loss of heterozygosity of Rat sarcoma (RAS) inhibitors result in frequent H-RAS activation in human HCC, particularly in patients with liver cirrhosis and shorter survival (20). Furthermore, Ras signaling activates NF-κB activity through the rapidly accelerated fibrosarcoma (Raf) pathway to mediate transformation of rat liver epithelial cells, which can be reversed by the inhibition of IκB kinase (IκK)-α (21).

Sorafenib (BAY 43-9006, Nexavar®, Bayer Inc., Leverkusen, North Rhine-Westphalia, Germany), a multi-kinase inhibitor mainly targeting RAF kinase, is the only drug approved by the Food and Drug Administration (FDA) for the systemic treatment of advanced HCC (22). NF-κB inhibition by sorafenib has been demonstrated in HCC cells (23, 24). However, the long-term observation of the anti-NF-κB effect of sorafenib in human HCC-bearing animals *in vivo* by molecular imaging, has not yet been reported as far as we are aware. In the present study, we generated a human hepatocellular carcinoma Huh7/NF-κB-*tk-luc2*/*rfp* tumor-bearing mouse model for assaying NF-κB activation and tumor growth *in vivo* by using multimodalities of molecular imaging (24), including micro single photon-emission computed tomography/computed tomography (microSPECT/CT), bioluminescent imaging (BLI), red fluorescent protein imaging (RFPI), and whole-body autoradiography. The tumor growth inhibition and downstream effectors of NF-κB were also assayed.

Materials and Methods

Cell culture. Three human HCC cell lines, Huh7, HepG2 and Hep3B, were used. Huh7 cell line was kindly provided by Dr. Jason Chia-Hsien Cheng at the Department of Radiation Oncology, National Taiwan University Hospital, Taipei, Taiwan. The other two were obtained from the American Type Culture Collection (ATCC, Gaithersburg, MD, USA). All three cell lines were maintained in Dulbecco's modified Eagle's medium (DMEM) supplemented with 10% fetal bovine serum (FBS), and cultured at 37˚C in a humidified incubator containing 5% CO_2. The Huh7/NFκB-*tk-luc2*/*rfp* stable clone (see below) was maintained under the same conditions except 500 μg/ml of G418 (Calbiochem, Darmstadt, Germany) was added to the medium.

Construction of NF-κB response element-driven herpes simplex virus (HSV) thymidine kinase (tk) and firefly luciferase (luc2) plasmid vector. Aquaspirillum serpens (Ase) I and *Bacillus megaterium* (Bmt) I restriction enzymes were used to a digest CMV-*ires-dsred2* vector (Clontech, Mountain View, USA), then blunted by Klenow enzyme to form pIres-*dsred2*. The NF-κB responsive element sequence was isolated from pNF-κB-*luc* vector (Clontech) with Micrococcus luteus (Mlu) I and *Haemophilus influenzae* Rd (Hind) III, then blunted by Klenow enzyme. The NF-κB responsive element sequence was ligated into pIres-*dsred2* to form the pNF-κB-*ires-dsred2* vector. The *luc2* DNA sequence was isolated from pGL4-luc2 (Promega, USA) with *Bacillus stearothermophilus* X (BstX) I and *Nocardia otitidis*-caviarum (Not) I, then blunted with Klenow enzyme. pNF-κB-*ires-dsred2* was digested with NotI and *Xanthomonas badrii* (Xba) I, then blunted with Klenow enzyme to form pNF-κB-*ires*. Isolated luc2 DNA sequence was inserted into pNF-κB-*ires* to form pNF-κB-*ires-luc2*. The HSV1-tk gene sequence was isolated from pORF-HSV1-tk (InvivoGen, San Diego, USA) with HindIII and *Escherichia coli* RY13 (EcoR) I, and then blunted with Klenow enzyme. Isolated HSV1-*tk* gene sequence was inserted upstream of *ires-luc2* in pNF-κB-*ires-luc2*, resulting in a final construction of pNF-κB-*tk-luc2* vector.

Establishment of Huh7/NF-κB-tk-luc2/red fluorescent protein gene (rfp) stable clone. The transfection of Huh7 cells was performed using jetPEI™ (Polyplus Transfection, Strasbourg, France). Huh7 cells (2×10^6) were seeded in a 10-cm diameter dish for 24 h before transfection. pNF-κB-*tk-luc2* vector (8 μg) and 16 μl of jetPEI™ solution were diluted with 500 μl and 484 μl of 145 mM NaCl, respectively, then immediately mixed together and incubated for 30 minutes at room temperature. The 1000 μl jetPEI™/DNA mixture was then added to the Huh7 cells in the 10 cm diameter dish, and incubated at 37˚C for 24 hours. Cells were then trypsinized and cultured with DMEM containing 1 mg/ml G418 supplemented with 10% FBS for two weeks. The surviving clones were isolated, and transferred to 96-well plates for growth. The expression of Luc2 protein in each clone was assayed using BLI. The recombinant bioluminescent cell clone was renamed as Huh7/NF-κB-*tk-luc2* cell line.

Both IκBα mutant vector (p-IκBαM; Clontech) and CAG promoter (composed of CMV enhancer and beta-actin promoter)-driven red fluorescent protein (RFP) vector (National RNAi Core Facility Platform, Academic Sinica, Taipei, Taiwan) were used to transfect Huh7/NF-κB-*tk-luc2* cell line with the same protocol as previously described. Two weeks after RFP vector transfection, cells with red fluorescence were sorted and isolated by flow cytometry. The isolated cells were transferred to 96-well plates for growth. The RFP expression in each clone was assayed using an IVIS50 Imaging System (Xenogen, Alameda, USA). Recombinant bioluminescent and red fluorescent cell clone was renamed as Huh7/NF-κB-*tk-luc2*/*rfp*.

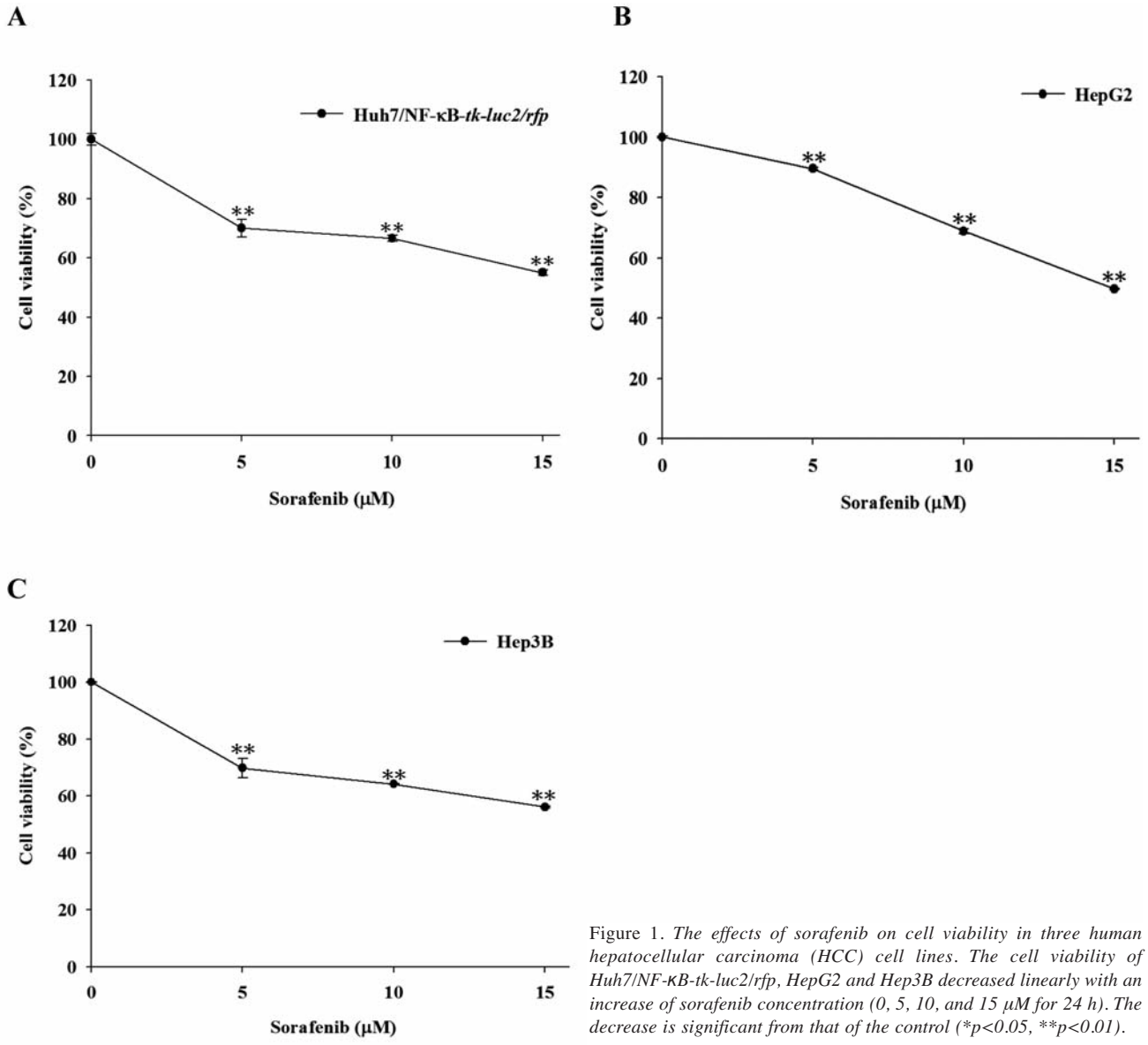

Figure 1. *The effects of sorafenib on cell viability in three human hepatocellular carcinoma (HCC) cell lines. The cell viability of Huh7/NF-κB-tk-luc2/rfp, HepG2 and Hep3B decreased linearly with an increase of sorafenib concentration (0, 5, 10, and 15 μM for 24 h). The decrease is significant from that of the control (*p<0.05, **p<0.01).*

Huh7/NF-κB-tk-luc2/rfp xenograft animal model. Male nude mice (n=10 per group, total 20 mice, 4-6 weeks old, National Laboratory Animal Center, Taipei, Taiwan) were injected subcutaneously in the right hind flank with 1×107 Huh7/NF-κB-*tk-luc2/rfp* cells. Tumor growth was monitored by caliper measurement twice a week and BLI once a week. Sorafenib treatment (20 mg/kg/day for 30 days by gavage) and the control group [phosphate buffer saline (PBS) in 1% Dimethyl sulfoxide (DMSO) by gavage daily] were initiated when the tumor volume reached approximately 50 mm^3. Mice were sacrificed at the end of the experiment (on day 30) for *ex vivo* western blotting and whole-body autoradiography. All animal study protocols were approved by the institutional animal care and use of National Yang-Ming University.

Cell viability assay. 3-(4,5-Dimethylthiazol-2-yl)-2,5-diphenyltetrazolium bromide (MTT, Sigma-Aldrich, St. Louis, USA) was dissolved in phosphate-buffered saline (145 mM NaCl, 1.4 mM KH_2PO_4, 4.3 mM Na_2HPO_4, and 2.7 mM KCl, pH 7.2). Huh7/NF-κB-*tk-luc2/rfp*, HepG2 and Hep3B cells were seeded into 96-well plates with 3×10^4 cells/well for 24 h before being treated with different concentrations of sorafenib (0, 5, 10, and 15 μM in 0.1% DMSO) for another 24 h. After washing with fresh medium, 100 μl of 5 mg/ml MTT solution was added to each well, and cells were incubated at 37˚C for 2 h. Then 100 μl DMSO was added to dissolve the MTT formazan, and the absorbance was determined with an ELISA reader (Power Wave X340, Bio-Tek Instrument Inc., Winooski, VT, USA) using a wavelength of 570 nm for excitation. The results are shown in Figure 1.

Electrophoretic mobility shift assay (EMSA). After treatment with 10 μM sorafenib for 48 h, nuclear fractions of Huh7/NF-kB-*tk-luc2/rf*p, HepG2 and Hep3B cells were isolated using Nuclear Extraction Kit (Chemicon International, Temecula, CA, USA). The NF-κB–DNA binding activity was evaluated using LightShift Chemiluminescent EMSA kit (Pierce, Rockford, IL, USA). The isolation and analysis procedures were followed the protocols provided with the kit. The following DNA sequences were synthesized for EMSA analysis. Sense: AGTTGAGGGGACTT TCCCAGGC and antisense: GCCTGGGAAAGTCCCCTCAACT for NF-κB. Nuclear extracts were incubated with the biotin-labeled DNA probe for 20 min at room temperature. The DNA–protein complex thus formed was separated from free oligonucleotides on a 5% polyacrylamide gel, then transferred to a nylon membrane and cross-linked with UV light. The membrane was incubated with streptavidin-horseradish peroxidase, and detected by enhanced chemiluminescence (ECL, Pierce, USA).

Western blotting. A total of 2×10^6 Huh7/NF-kB-tk-luc2/rfp, HepG2 and Hep3B cells were seeded into 10-cm diameter dishes for 24 h prior to treatment with different concentrations of sorafenib. In addition, cells were treated with 10 μM sorafenib for 0, 24 and 48 h, then lysed with 100 μl lysis buffer [50 mM Tris-HCl (pH 8.0), 120 mM NaCl, 0.5% NP-40, 1 mM phenylmethane-sulfonylfluoride]. Total proteins (40 μg) were separated by 10% sodium dodecyl sulfate–polyacrylamide gel electrophoresis (SDS–PAGE), then transferred to a polyvinylidene difluoride membrane (Millipore, Billerica, MA, USA), blocked with 5% non-fat milk in TBS–Tween buffer (0.12 M Tris-base, 1.5 M NaCl, and 0.1% Tween20) for 1 h at room temperature, then incubated with the appropriate primary antibody (VEGF, MMP-9, XIAP, BCL-2, cyclin-D1, and β-actin, respectively; Millipore) overnight at 4˚C, followed by incubation with secondary peroxidase-conjugated anti-rabbit antibody for 30 min at room temperature. The expressions of proteins were determined by ECL (Millipore). The ImageJ software (National Institutes of Health, Bethesda, MD, USA) was used for the quantitative analysis.

Ex vivo western blotting. Mice were sacrificed on day 30 post daily sorafenib treatment. Tumors were removed for protein extraction using the T-PER kit (Thermo Scientific, Rockford, IL, USA). Equal amounts of protein (40 μg) were loaded on SDS-PAGE for electrophoresis, then transferred to nitrocellulose membranes. The membranes were incubated with primary antibodies specific for VEGF, MMP-9, XIAP, cyclin-D1 and cleaved caspase-3, followed by incubation with horseradish peroxidase-conjugated secondary antibodies. Protein expression was determined by ECL. All reagents and antibodies were purchased from Millipore, except XIAP, which was purchased from Abcam, Cambridge, UK.

Therapeutic evaluation of sorafenib by molecular imaging in vitro and in vivo. The procedures for each imaging modality were described in our previous study (25), and are summarized briefly in the following.

BLI. BLI is used for monitoring of the NF-κB activation in Huh7/NF-κB-*tk-luc2/rfp* cells and animal tumor xenografts. For BLI *in vitro*, 3×10^4 Huh7/NF-κB/*tk-luc2/rfp* cells were cultured in a 96-well plate for 24 h, then treated with different concentrations of sorafenib (0, 5, 10, and 15 μM in 0.1% DMSO) for 3 h. To each well was added 100 μl of 500 μM D-luciferin (Xenogen) for imaging. For *in vivo* BLI, mice received 150 mg/kg D-luciferin *via* intra-peritoneal injection and were anesthetized using 1-3% isoflurane for 15 min before imaging. The photons emitted from the cells or tumors *in vivo* were detected by an IVIS50 Imaging System (Xenogen). All images were acquired 1 and 5 min for *in vitro* and *in vivo*, respectively. Regions of interest (ROIs) of the images were drawn in each well and around the tumor, and quantified as photons/second using Living Image software (Version 2.20; Xenogen).

RFPI. RFPI was used for monitoring viable tumor cell growth in the Huh7/NFκB-*tk-luc2/rfp* xenograft mouse model. The photons emitted from RFP in the tumors were detected by IVIS50 Imaging System. All images were acquired for 30 sec. ROIs of the images were drawn around the tumor and quantified as photons/s using the Living Image software (Version 2.20, Xenogen, USA).

Micro-SPECT/CT using ^{123}I-1-(2-deoxy-2-fluoro-1-D-arabinofuranosyl)-5-iodouracil (^{123}I-FIAU). ^{123}I-FIAU combined with microSPECT/CT was used to monitor NF-κB–DNA binding activity in the Huh7/NF-kB-*tk-luc2/rfp* xenograft mouse model. On day 7 post-sorafenib treatment, mice were injected intravenously (*i.v.*) with 3.7×10^7 Bq/0.1 ml ^{123}I-FIAU. The whole-body images of mice were obtained by microSPECT/CT scanner (FLEX Triumph; GE Medical Systems Waukesha, Wl, USA). The image acquisition time was 30 min.

Whole-body autoradiography. Mice were injected *i.v.* with 100 μCi/0.2 ml ^{131}I-FIAU on day 30 post-sorafenib treatment, and sacrificed 24 h later for whole-body autoradiography as previously described (26). Frontal sectioning was performed at a thickness of 20 μm at –20˚C with a cryostat microtome (Bright Instrument Company Ltd., Huntingdon, UK). Sections were placed on the imaging plate (BAS-SR2040; Fuji Photo Film, Tokyo, Japan) in the cassette (2040; Fuji Photo Film). After exposure, the imaging plate was assayed with an FLA5000 reader (Fuji Photo Film) to acquire the phosphor image. Reading parameters of the reader were the following: resolution of 10 μm, gradation of 16 bits, 635 nm laser light, and 800 V of photomultiplier tube.

Statistical analysis. Student's *t*-test was used to evaluate the significance of the differences. Standard error of the mean is depicted as the error bar in all figures.

Results

Multimodalities of molecular imaging for Huh7/NF-κB-tk-luc2/rfp xenograft-bearing mice. The Huh7/NF-κB-*tk-luc2/rfp* cells were transfected with two kinds of vectors, as shown in Figure 2A. One is driven by NF-κB-responsive elements and carries two reporter genes, *tk* and *luc2*, for real-time monitoring of NF-kB activity *in vivo* with BLI and microSPECT/CT. The other CAG-*rfp* vector is driven by CMV enhancer and beta-actin promoter to express the *RFP* gene for distinguishing the viable from non-viable cells by RFPI. The photon flux obtained from RFPI is well-correlated with the cell number in the dish, as shown in Figure 2B.

Sorafenib inhibits NF-κB activation and effector proteins expression. Cell viability with MTT assay and RFP expression levels with RFPI were not significant different in

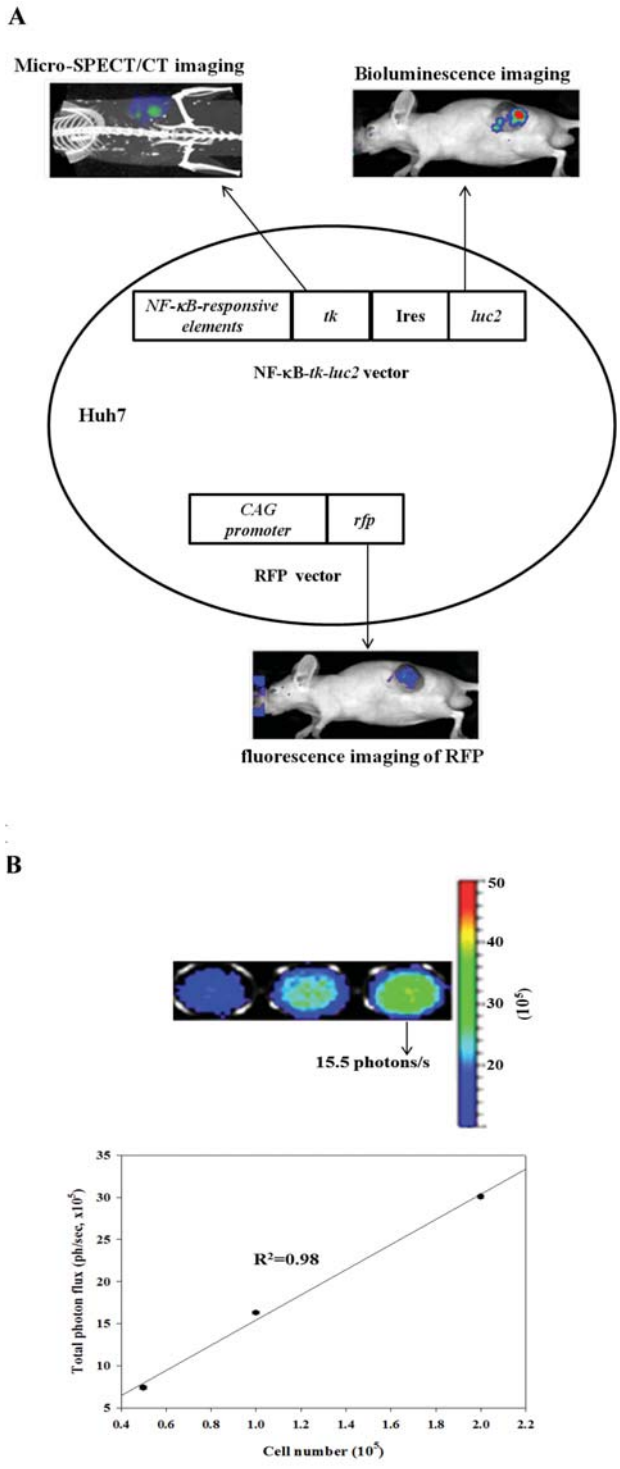

Figure 2. *The strategy for evaluation of nuclear factor-κB (NF-κB) activation and red fluorescence protein (RFP) expression in Huh7/NF-κB-tk-luc2/rfp tumor-bearing mice with multimodalities of molecular imaging. A: Multimodalities of molecular imaging including microSPECT/CT, BLI, and RFPI from the same mouse carrying triple-reporter genes are shown. B: Total photon flux emitted from the expression of rfp gene in Huh7/NF-κB-tk-luc2/rfp cells is the function of the cell number with* R^2*=0.98.*

Huh7/NF-κB-*tk-luc2*/*rfp* cells treated with 0-15 μM sorafenib (Figure 3A and B). Notably, the relative NF-κB activity of Huh7/NF-κB-*tk-luc2*/*rfp* cells assayed by BLI was significantly suppressed by sorafenib in a dose-dependent manner (Figure 3C). Similar results were also found with EMSA, in which NF-κB–DNA binding activity was inhibited in three human HCC cell lines treated with 10 μM sorafenib for 48 h (Figure 3D). Expressions of NF-κB-regulated downstream effector proteins (VEGF, MMP-9, XIAP, BCL-2, and cyclin-D1, respectively) were down-regulated by 10 μM sorafenib treatment for both 24 and 48 h (Figure 4A). In addition, significant inhibition of NF-κB activation in p-IκBαM super repressor–transfected Huh7/NF-κB-*tk-luc2* cells was found, as compared with that of the empty vector (E vector)–transfected cells, which further confirmed the inhibitory effects of sorafenib on NF-κB activation and the expression of downstream proteins (Figure 4B).

Sorafenib suppresses constitutively activated NF-κB activity and inhibits tumor growth in Huh7/NF-κB-tk-luc2/rfp tumor-bearing mice. Huh7/NF-κB-tk-luc2/rfp tumor-bearing mice treated with 20 mg/kg/day sorafenib were imaged once per week with BLI and RFPI. Both NF-κB activation and viable tumor cell number increment, as shown by RFPI, were significantly inhibited by sorafenib treatment throughout the experimental period, as compared with that of vehicle-treated (PBS with 1% DMSO by daily gavage) mice (Figure 5A). The quantification of the tumor images in Figure 5A is shown in Figure 5B. The expression of NF-κB effector proteins in the tumors obtained from day 30 post-vehicle and -sorafenib treatments, respectively, are shown in Figure 5C. These effector proteins were also suppressed by sorafenib. Significant tumor growth inhibition in sorafenib-treated mice as compared with that of the vehicle-treated ones with digital caliper measurement is shown in Figure 5D. The relative photon fluxes obtained from RFPI and BLI, which represent the viable cells and NF-κB activation, respectively, decreased after sorafenib treatment by 50 to 65% (Figure 5E), and 87.5 to >90% (Figure 5F), suggesting that NF-κB activation is suppressed in viable HCC cells by sorafenib. In addition, microSPECT/CT performed on days 7 and 30, respectively, post-sorafenib treatment showed a similar pattern of non-homogenous distribution of NF-κB signals to that obtained from BLI, but not for images obtained from RFPI (Figure 6A). Similarly, the uptake of ^{131}I-FIAU in tumors by whole-body autoradiography performed at both time points also gave results consistent with those by microSPECT/CT and BLI (Figure 6B).

Discussion

Recurrent new lesions often result in treatment failure in most patients with HCC after surgical resection or local radiotherapy due to the tumorigenic environment of the

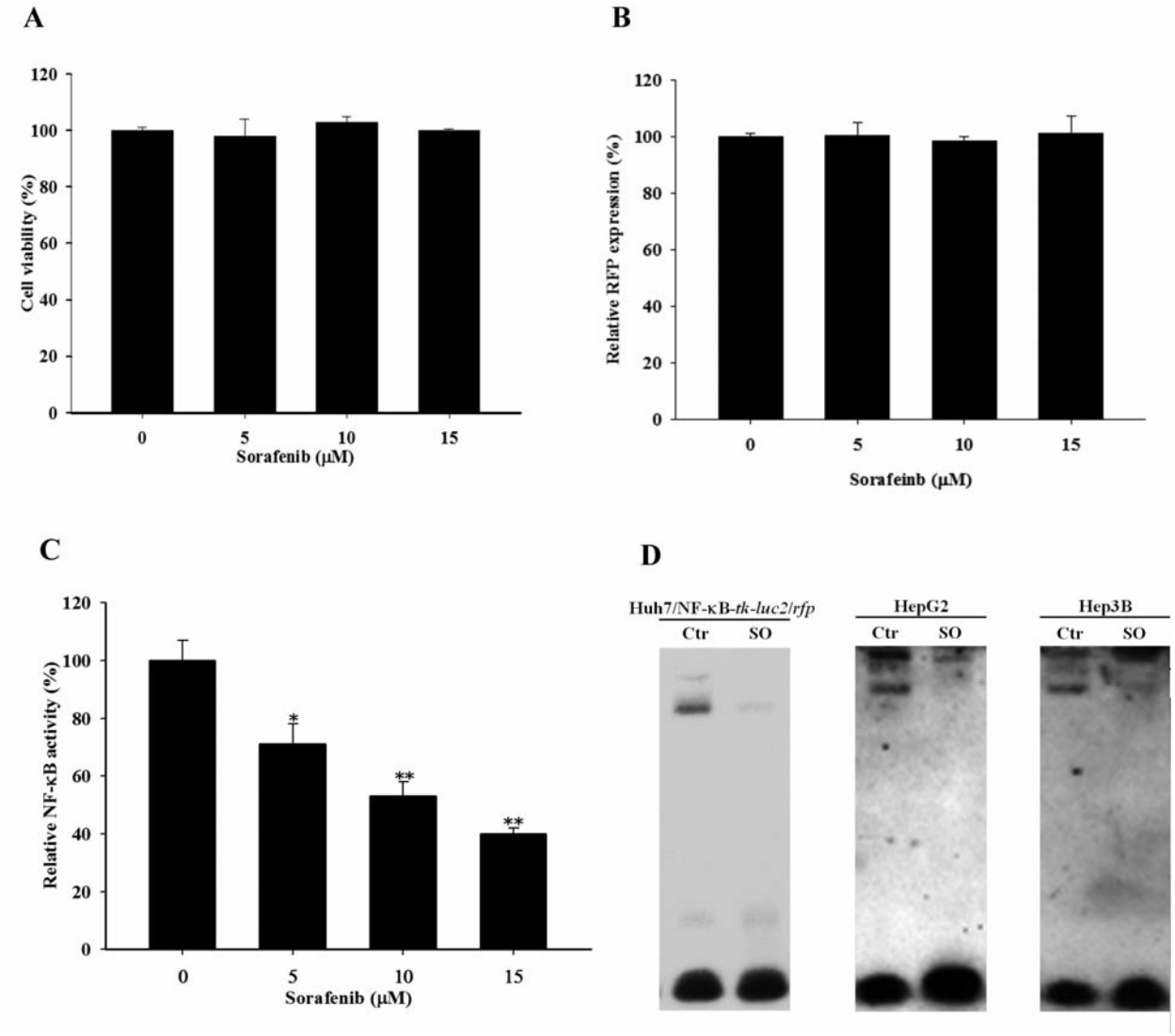

Figure 3. *Sorafeinb reduces the expression of nuclear factor-κB (NF-κB)-regulated downstream proteins via inhibition of NF-κB activation. No significant changes were found in cell viability (A) or RFP expression (B) for the same Huh7/NF-κB-tk-luc2/rfp cell population treated with 5-15 μM sorafenib for 3 h, then assayed with 3-(4,5-Dimethylthiazol-2-yl)-2,5-diphenyltetrazolium bromide (MTT) and IVIS50 optical system, respectively. C: NF-κB activation was significantly reduced by treatment with 5-15 μM sorafenib for 3 h as shown with bioluminescent imaging (BLI). D: The NF-κB–DNA binding activity was inhibited in three human hepatocellular carcinoma (HCC) cell lines treated with 10 μM sorafenib (So) for 48 h, and assayed with Electrophoretic mobility shift assay (EMSA).*

whole liver accompanied by chronic hepatitis (2, 13). The NF-κB signaling pathway has been linked to radio- and chemo-resistance of inflammatory-related oncogenesis, and to increased proliferation, invasion/metastasis and decreased apoptosis in HCC cell lines (5, 6). It has been suggested that radiotherapy combined with other strategies is capable of suppressing NF-κB signal transduction to inhibit radiation-induced MMP-9 expression *via* phosphatidylinositol-3-kinase (PI3K)/AKT/NF-κB pathway in human HCC (15). We also reported that sorafenib-sensitized human colorectal carcinoma to radiation *via* suppression of NF-κB–DNA binding activity and its downstream effectors induced by ionizing radiation. In addition, the synergistic effect was also found with combination of sorafenib and radiation in a tumor-bearing animal model (27).

The NF-κB/*luc* system has been used as a platform for rapid screening of drugs with the potential to inhibit NF-κB activity in human HepG2 hepatoma-bearing mice (19). Here, we further improved the system with dual reporter genes (*tk-luc2*) to combine multimodalities of molecular imaging for the measurement of NF-κB activity. In this study, we demonstrated a simultaneous imaging of the temporal change

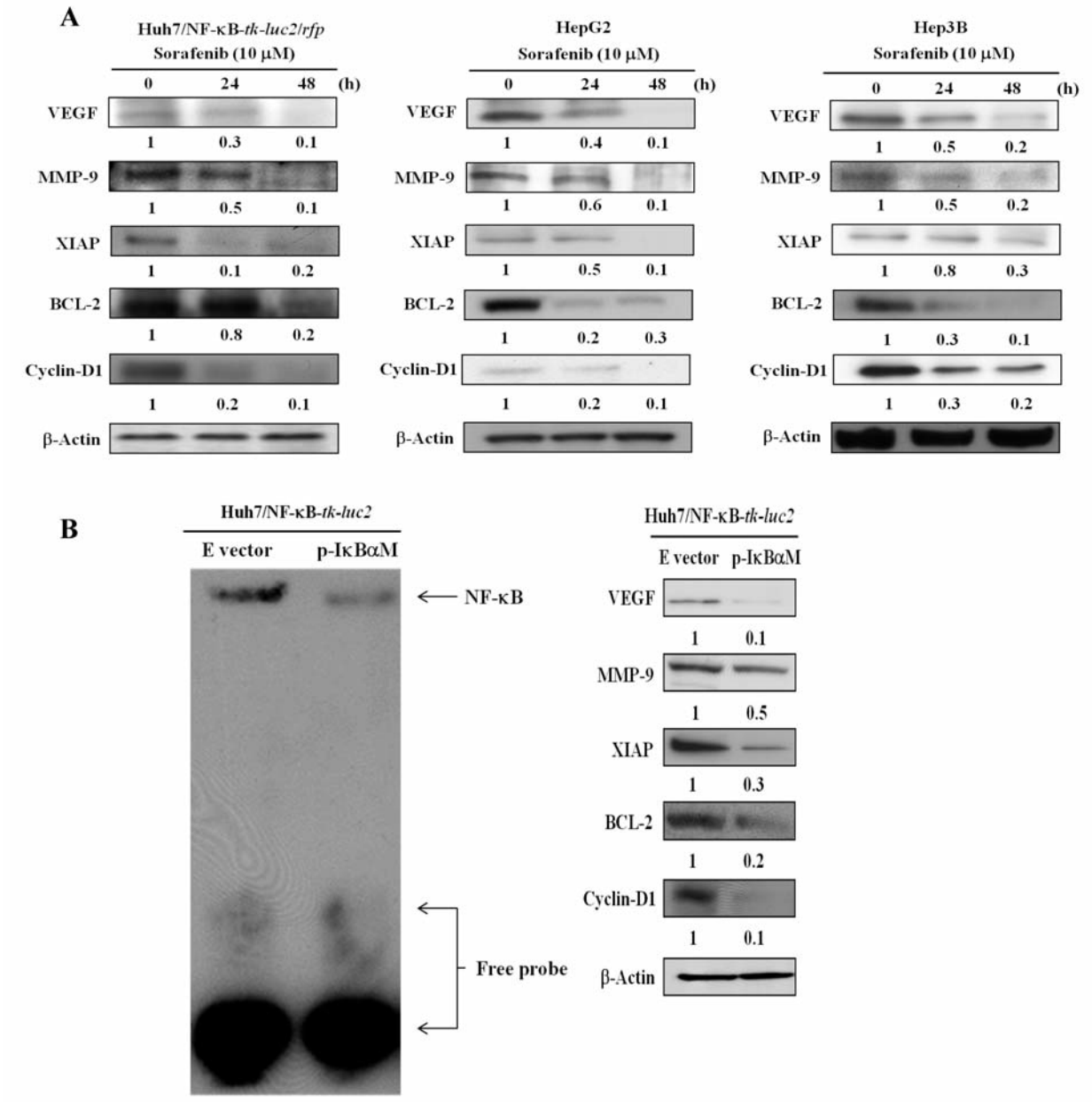

Figure 4. *The expressions of nuclear factor-κB (NF-κB)-regulated downstream proteins in three human hepatocellular carcinoma (HCC) cell lines are suppressed by sorafenib and inhibitor of kappaB-α mutant vector (p-IκBαM), respectively. A: Cells were treated with 10 μM sorafenib for 24 and 48 h, respectively, then assayed with western blotting. The expression of vascular endothelial growth factor (VEGF), matrix metalloproteinase-9 (MMP-9), X-linked inhibitor of apoptosis protein (XIAP), B-cell lymphoma-2 (BCL-2), and cyclin-D1 was suppressed in all three human hepatocellular carcinoma (HCC) cell lines. B: Huh7/NF-κB-tk-luc2 cells were transfected with p-IκBαM vector, then assayed by Electrophoretic mobility shift assay (EMSA) and western blotting. Left: NF-κB–DNA binding activity was inhibited in p-IκBαM-transfected cells. Right: The expressions of NF-κB-regulated downstream proteins were inhibited in p-IκBαM-transfected cells. *p<0.05 and **p<0.01 as compared with that of the vehicle-treated control.*

of NF-κB activation with BLI and of actively-growing tumor cells with RFPI in the same Huh7/NF-κB-*tk-luc2/rfp* tumors of the animal (Figure 5B). In addition, NF-κB activation is heterogeneously-distributed in the tumors, and NF-κB expression fluctuates with time (Figure 5A). Notably, the increase of NF-κB imaging signal coincides with the tumor growth (Figures 5D and 5F), suggesting that the expression of NF-κB is constitutively activated in HCC, and this may also occur in other tumor types. This finding may also suggest that NF-κB expression in the tumor biopsy of a patient examined

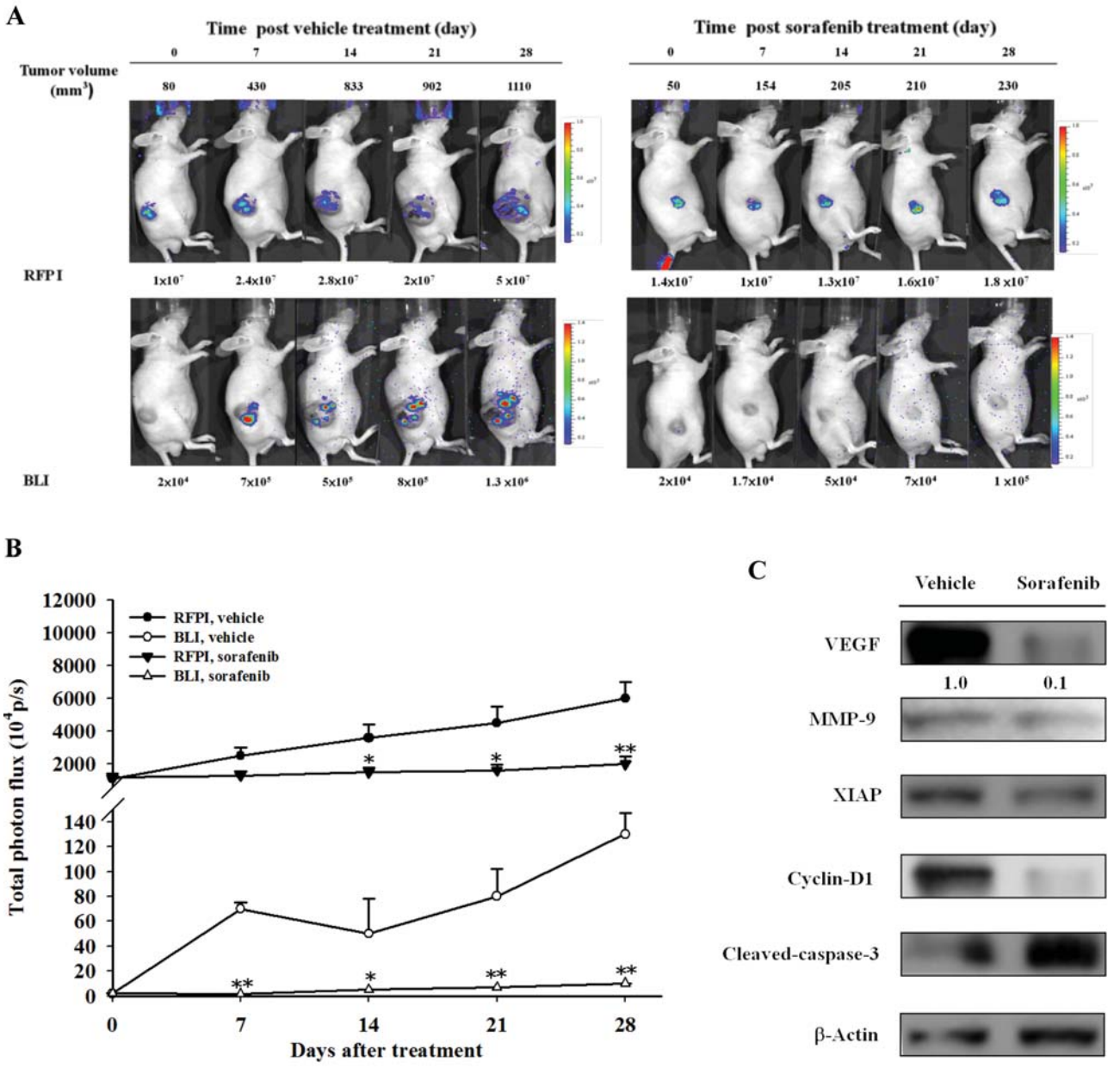

Figure 5. *Continued*

with IHC staining only represents regional expression and a certain progression time point of the tumor, and does not reflect the whole picture of the NF-κB expression in that tumor. As such, IHC staining of the tumor biopsy from a patient may not always be suitable as a predictive assay of the theranostic outcome. In addition, the tumor is capable of growing fast in the absence of an effective chemotherapeutic drug to inhibit the NF-κB signaling cascade (see vehicle treatment in Figures 5A and B). Pathological examination further shows the inhomogeneous distribution of necrosis in the tumors (Figure 7), which is consistent with the image pattern of the RFPI assay.

Sorafenib suppresses NF-κB activation and its downstream effector proteins both *in vitro* and *in vivo*. Nevertheless, the optimal level for NF-κB activity remains unclear and is worthy of being investigated further, since the complete blockade of physiologic NF-κB activity raises the concern of cancer escape from immune surveillance (17, 28). Tumor-bearing mice

Figure 5 Continued

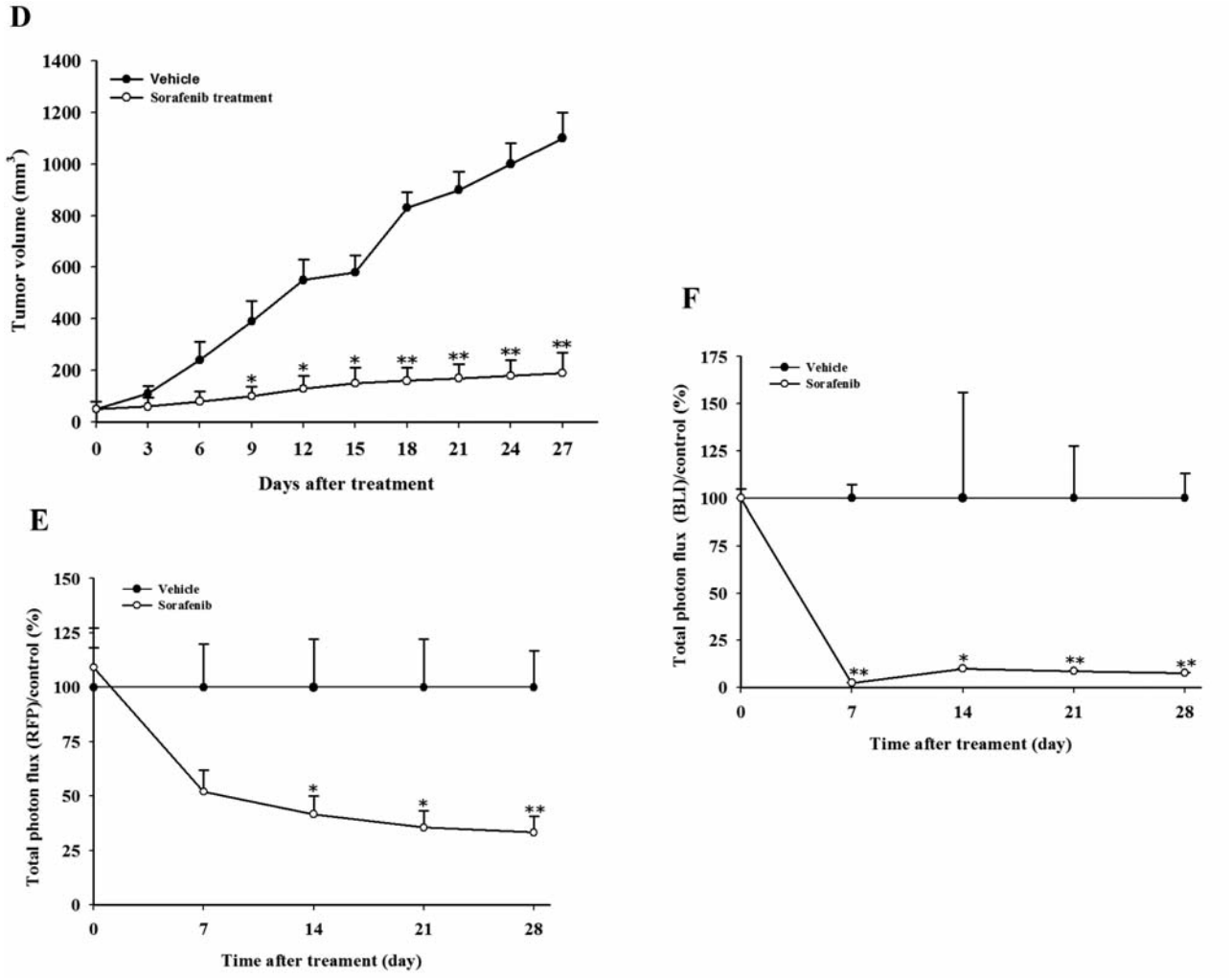

Figure 5. *Tumor regression is correlated with the suppression of nuclear factor-κB (NF-κB) after sorafenib treatment by multimodalities of molecular imaging in Huh7/NF-κB-tk-luc2/rfp tumor-bearing mice. A: The photon fluxes obtained from bioluminescence imaging (BLI) and red fluorescent protein imaging (RFPI) in Huh7/NF-κB-tk-luc2/rfp tumor-bearing mice treated with the vehicle and sorafenib (20 mg/kg/d), respectively, are shown. B: Photon fluxes from RFPI and BLI shown in (A) were quantified and compared. Photon fluxes were significantly lower in sorafenib-treated mice as compared with that of the vehicle-treated mice; n=4 in each group; *p<0.05 and **p<0.01 as compared with that of the vehicle-treated control. C: The expressions of NF-κB effector proteins in the tumors obtained from day 30 post-vehicle and sorafenib treatments, respectively, were assayed with ex vivo western blotting. The expression of vascular endothelial growth factor (VEGF), matrix metalloproteinase-9 (MMP-9), X-linked inhibitor of apoptosis protein (XIAP), cyclin-D1, and cleaved caspase-3 was suppressed in sorafenib-treated Huh7/NF-kB-tk-luc2/rfp cells. D: Tumor growth and inhibition as assayed with digital caliper; n=5 in each group, *p<0.05 and **p<0.01, as compared with that of the vehicle-treated control. E: The change of photon flux ratio byRFPI under sorafenib treatment as compared with that of the control. The relative photon flux under sorafenib treatment was continuously decreased. (F) The change of photon fluxes ratio of BLI in sorafenib treatment as compared with that of the control. The ratios of photon fluxes rate of the sorafenib treatment were significantly reduced.*

treated with sorafenib exhibited very low or negligible NF-κB signals by BLI as compared with that of the controls throughout the experimental period of 30 days (Figure 6A). These results may provide a rationale for concurrent treatment of HCC with radiotherapy and sorafenib, since NF-κB activity could be suppressed during the course of radiotherapy, which usually lasts for 3 to 6 weeks (3). One of the pro-survival signals induced by ionizing radiation leading to radioresistance in cancer cells is through the expression of NF-κB and its regulated downstream proteins, such as XIAP and BCL-2, to inhibit mitochondria-dependent and caspase-3-induced apoptosis (29). Sorafenib is able to increase the expression of

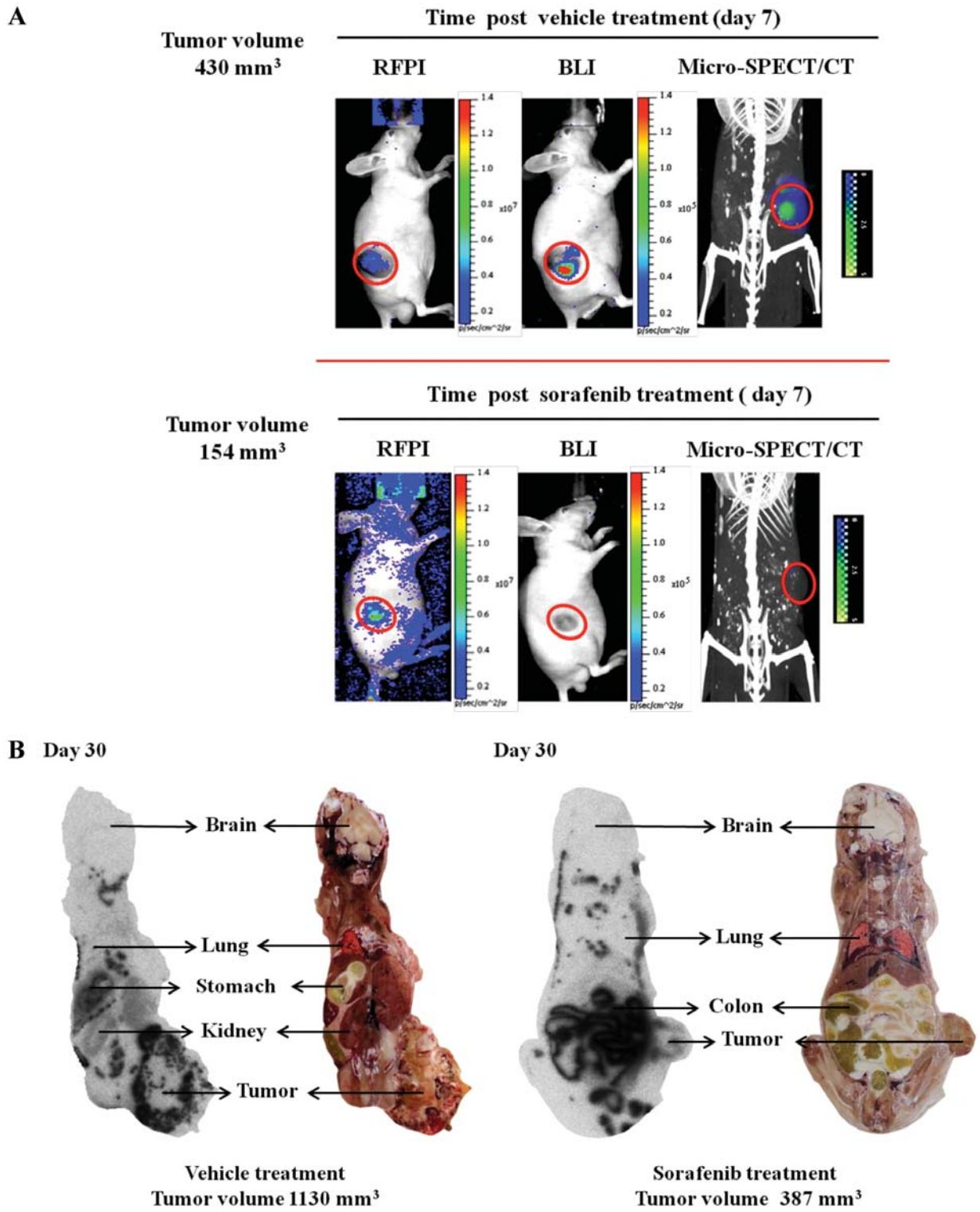

Figure 6. *Tumor volumes as monitored by multimodalities of molecular imaging on days 7 and 30 were compared. A: Tumor volume measured with a caliper is shown in the Figure. Red fluorescent protein imaging (RFPI), bioluminescent imaging (BLI), and micro single-photon emission computed tomography/computed tomography (SPECT/CT) images were performed on day 7 post-sorafenib treatment (20 mg/kg/d). Sorafenib-treated mice are shown to have lower photon signals by BLI, RFPI, and micro-SPECT/CT as compared with those of the vehicle-treated control. B: Whole-body autoradiography was performed after mice were injected i.v. with 3.7×10^6 Bq/0.2 ml ^{131}I-FIAU on day 30. The tumor of the vehicle-treated control is lager with higher uptake of 131I-FIAU, as compared with that of the sorafenib-treated mouse.*

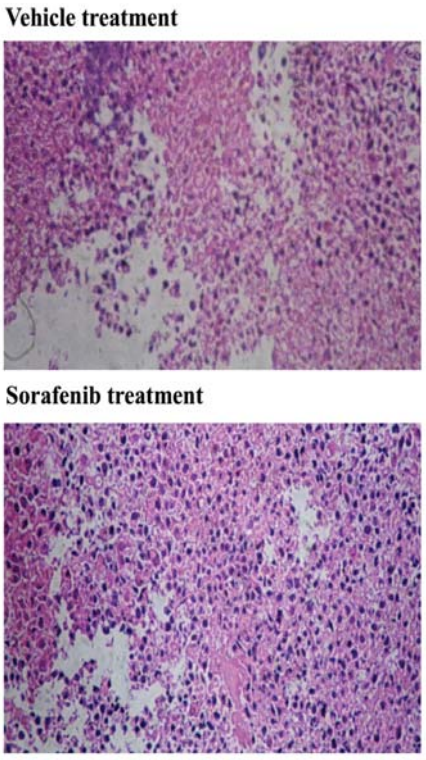

Figure 7. *Pathological examination of tumor tissues obtained from the vehicle- and sorafenib-treated Huh7/NF-κB-tk-luc2/rfp tumor-bearing mice on day 30 by H&E staining (×160). Inhomogeneous distribution of necrosis in the tumors was observed in the vehicle-treated group.*

cleaved caspase-3 (Figure 5C). The results suggest that sorafenib may reduce or inhibit anti-apoptotic signals through the suppression of NF-κB. As a result, sorafenib may be a better choice of chemotherapy to be combined with radiotherapy, which often increases NF-κB (15, 27), in order to reduce radioresistance and augment the therapeutic effect in HCC and other tumor types. However, further clinical trials combining sorafenib with radiotherapy or as an adjuvant treatment after curative resection or ablative treatment are needed to validate this. In addition, the feasibility of using an NF-κB image-guided approach to identify those patients with increased NF-κB activity remains to be explored, and may be beneficial for clinical application.

Conclusion

Simultaneous molecular imaging of the temporal change of NF-κB activity and the viable tumor cells in the same Huh7/NF-κB-*tk-luc2*/*rfp* tumors of an animal may provide a useful platform for monitoring tumor progression, therapeutic efficacy of chemotherapeutic drugs, such as sorafenib, and actually reflects the real situation of NF-κB activity and viable tumor cells at the time of imaging.

Acknowledgements

This study was supported by grant NSC 101-2623-E-010-005-NU from the National Science Council, Taipei, Taiwan. The imaging facilities were supported by the MAGIC core of the National Research Program for Genomic Medicine (NRPGM), National Science Council, Taipei, Taiwan.

References

1 Ferlay J, Shin HR, Bray F, Forman D, Mathers C and Parkin DM: Cancer Incidence and Mortality Worldwide: IARC CancerBase No. 10. Ver.1.2. http://globocan.iarc.fr. Last accessed 29th, January, 2012.
2 El-Serag HB: Hepatocellular carcinoma. N Engl J Med *365*: 1118-1127, 2011.
3 Feng M and Ben-Josef E: Radiation therapy for hepatocellular carcinoma. Semin Radiat Oncol *21*: 271-277, 2011.
4 Koehler BC, Urbanik T, Vick B, Boger RJ, Heeger S, Galle PR, Schuchmann M and Schulze-Bergkamen H: TRAIL-induced apoptosis of hepatocellular carcinoma cells is augmented by targeted therapies. World J Gastroenterol *15*: 5924-5935, 2009.
5 Li F and Sethi G: Targeting transcription factor NF-κB to overcome chemoresistance and radioresistance in cancer therapy. Biochim Biophys Acta *1805*: 167-180, 2010.
6 Wu JM, Sheng H, Saxena R, Skill NJ, Bhat-Nakshatri P, Yu M, Nakshatri H and Maluccio MA: NF-κB inhibition in human hepatocellular carcinoma and its potential as adjunct to sorafenib based therapy. Cancer Lett *278*: 145-155, 2009.
7 Pikarsky E, Porat RM, Stein I, Abramovitch R, Amit S, Kasem S, Gutkovich-Pyest E, Urieli-Shoval S, Galun E and Ben-Neriah Y: NF-κB functions as a tumour promoter in inflammation-associated cancer. Nature *431*: 461-466, 2004.
8 Ozaki I, Zhang H, Mizuta T, Ide Y, Eguchi Y, Yasutake T, Sakamaki T, Pestell RG and Yamamoto K: Menatetrenone, a vitamin K2 analogue, inhibits hepatocellular carcinoma cell growth by suppressing cyclin D1 expression through inhibition of nuclear factor kappaB activation. Clin Cancer Res *13*: 2236-2245, 2007.
9 Kang YH, Park MY, Yoon DY, Han SR, Lee CI, Ji NY, Myung PK, Lee HG, Kim JW, Yeom YI, Jang YJ, Ahn DK and Song EY: Dysregulation of overexpressed IL-32α in hepatocellular carcinoma suppresses cell growth and induces apoptosis through inactivation of NF-κB and BCL-2. Cancer Lett *318*: 226-233, 2012.
10 Shyu MH, Kao TC and Yen GC: Oleanolic acid and ursolic acid induce apoptosis in HuH7 human hepatocellular carcinoma cells through a mitochondrial-dependent pathway and down-regulation of XIAP. J Agric Food Chem *58*: 6110-6118, 2010.
11 Xiang Z, Zeng Z, Tang Z, Fan J, Sun H, Wu W and Tan Y: Increased expression of vascular endothelial growth factor-C and nuclear CXCR4 in hepatocellular carcinoma is correlated with lymph node metastasis and poor outcome. Cancer J *15*: 519-525, 2009.
12 Claudio PP, Russo G, Kumar CA, Minimo C, Farina A, Tutton S, Nuzzo G, Giuliante F, Angeloni G, Maria V, Vecchio FM, Campli CD and Giordano A: pRb2/p130, vascular endothelial growth factor, p27(KIP1), and proliferating cell nuclear antigen expression in hepatocellular carcinoma: Their clinical significance. Clin Cancer Res *10*: 3509-3517, 2004.

13 Meng F, Henson R and Patel T: Chemotherapeutic stress selectively activates NF-κB-dependent AKT and VEGF expression in liver cancer-derived endothelial cells. Am J Physiol Cell Physiol *293*: C749-760, 2007.

14 Hsiang CY, Wu SL, Chen JC, Lo HY, Li CC, Chiang SY, Wu HC and Ho TY: Acetaldehyde induces matrix metalloproteinase-9 gene expression *via* nuclear factor-κB and activator protein 1 signaling pathways in human hepatocellular carcinoma cells: Association with the invasive potential. Toxicol Lett *171*: 78-86, 2007.

15 Cheng JC, Chou CH, Kuo ML and Hsieh CY: Radiation-enhanced hepatocellular carcinoma cell invasion with MMP-9 expression through PI3K/AKT/NF-κB signal transduction pathway. Oncogene *25*: 7009-7018, 2006.

16 Lee KW, Kang NJ, Kim JH, Lee KM, Lee DE, Hur HJ and Lee HJ: Caffeic acid phenethyl ester inhibits invasion and expression of matrix metalloproteinase in SK-Hep1 human hepatocellular carcinoma cells by targeting nuclear factor kappa B. Genes Nutr *2*: 319-322, 2008.

17 Liu YC, Chiang IT, Hsu FT and Hwang JJ: Using NF-κB as a molecular target for theranostics in radiation oncology research. Expert Rev Mol Diagn *12*: 139-146, 2012.

18 Liu Z, Cheng M and Cao M: Potential targets for molecular imaging of apoptosis resistance in hepatocellular carcinoma. Biomed Imaging Interv J *7*: e5, 2011.

19 Chang TJ, Chang YJ, Ho TY, Hsiang CY, Yu CY, Lee TW, Lin WJ and Chang CH: Noninvasive bioluminescent and microPET imaging for the regulation of NF-κB in human hepatoma-bearing mice. Anticancer Res *29*: 987-994, 2009.

20 Calvisi DF, Ladu S, Gorden A, Farina M, Conner EA, Lee JS, Factor VM and Thorgeirsson SS: Ubiquitous activation of RAS and JAK/STAT pathways in human HCC. Gastroenterology *130*: 1117-1128, 2006.

21 Arsura M, Mercurio F, Oliver AL, Thorgeirsson SS and Sonenshein GE: Role of the IkappaB kinase complex in oncogenic Ras- and Raf-mediated transformation of rat liver epithelial cells. Mol Cell Biol *20*: 5381-5391, 2000.

22 Wilhelm S, Carter C, Lynch M, Lowinger T, Dumas J, Smith RA, Schwartz B, Simantov R and Kelley S: Discovery and development of sorafenib: a multikinase inhibitor for treating cancer. Nat Rev Drug discov *5*: 835-844, 2006.

23 Chiang IT, Liu YC, Wang WH, Hsu FT, Chen HW, Lin WJ, Chang WY and Hwang JJ: Sorafenib inhibits TPA-induced MMP-9 and VEGF expression *via* suppression of ERK/NF-κB pathway in hepatocellular carcinoma cells. In Vivo *26*: 671-681, 2012.

24 Urbanik T, Kohler BC, Boger RJ, Worns MA, Heeger S, Otto G, Hovelmeyer N, Galle PR, Schuchmann M, Waisman A and Schulze-Bergkamen H: Down-regulation of CYLD as a trigger for NF-κB activation and a mechanism of apoptotic resistance in hepatocellular carcinoma cells. Int J Oncol *38*: 121-131, 2011.

25 Chang YF, Lin YY, Wang HE, Liu RS, Pang F and Hwang JJ: Monitoring of tumor growth and metastasis potential in MDA-MB-435s/tk-luc human breast cancer xenografts. Nucl Instr Meth Phys Res A *571*: 155-159, 2007.

26 Lin KJ, Ye XX, Yen TC, Wey SP, Tzen KY, Ting G and Hwang JJ: Biodistribution study of [(123)I] ADAM in mice: Correlation with whole body autoradiography. Nucl Med Biol *29*: 643-650, 2002.

27 Kuo YC, Lin WC, Chiang IT, Chang YF, Chen CW, Su SH, Chen CL and Hwang JJ: Sorafenib sensitizes human colorectal carcinoma to radiation *via* suppression of NF-κB expression *in vitro* and *in vivo*. Biomed Pharmacother *66*: 12-20, 2012.

28 Kim R, Emi M and Tanabe K: Cancer immunoediting from immune surveillance to immune escape. Immunology *121*: 1-14, 2007.

29 Magne N, Toillon RA, Bottero V, Didelot C, Houtte PV, Gerard JP and Peyron JF: NF-κB modulation and ionizing radiation: Mechanisms and future directions for cancer treatment. Cancer Lett *231*: 158-168, 2006.

Received January 25, 2013
Revised March 13, 2013
Accepted March 14, 2013